Ultramicroscopy 110 (2010) 971–980

Contents lists available at ScienceDirect

Ultramicroscopy

journal homepage: www.elsevier.com/locate/ultramic

Energy resolution of an Omega-type monochromator and imaging properties of the MANDOLINE filter

Erik Essers [a,*], Gerd Benner [a], Thilo Mandler [a], Stefan Meyer [a], Dieter Mittmann [a], Michael Schnell [a], Rainer Höschen [b]

[a] Carl Zeiss NTS GmbH, Carl-Zeiss-Strasse 56, 73447 Oberkochen, Germany
[b] Max Planck Institute for Metals Research, Heisenbergstr. 3, 70569 Stuttgart, Germany

ARTICLE INFO

Keywords:
Monochromator
Energy resolution
EELS
Energy-filtered imaging
Imaging energy filter
MANDOLINE filter
Corrected OMEGA filter
Transmissivity

ABSTRACT

We report on the energy resolution properties of an Omega-type monochromator. In a TEM/STEM setup with a MANDOLINE filter and extreme stability of the high voltage and the filter current, an energy resolution of 43 meV for 0.1 s exposure time and 87 meV for 100 s exposure time was measured at 200 kV with 40 meV monochromator slit width. The monochromized zero-loss peaks are additionally characterized by their edge steepness. Moreover a drop in the monochromized zero-loss peak by 10^3 after 260 meV can be obtained even without deconvolution. For small fields of view, the energy resolution mostly does not depend on the MANDOLINE filter. With the Corrected OMEGA filter an energy resolution of 41 meV was measured for 0.03 s exposure time at 200 kV with 30 meV monochromator slit width and 77 meV for 50 s exposure time at 80 kV with 40 meV monochromator slit width. Furthermore, the MANDOLINE filter's setup and imaging properties are presented such as isochromaticity (<5 meV) and transmissivity ($T_{(1\,eV)}$=17,400 nm^2), which set a new standard for imaging energy filters and allow EFTEM spectrum imaging with energy windows ≤ 200 meV and reasonable fields of view.

1. Introduction

In recent years monochromators have become commercially available for TEM/STEMs, thereby opening up many new possibilities for analytical investigations. Nevertheless the attainable energy resolution is usually still above 100 meV. A further improvement of the energy resolution by an optimized instrumental setup would be very interesting for a further exploration of new fields of research, especially in the low-loss region of EEL spectra. Besides the improved energy resolution, another advantage of monochromized spectra is the strongly reduced tail of the zero-loss peak (ZLP), thus giving access to the region of the band gap directly behind the monochromized ZLP. Nevertheless improved band gap measurements demand for a further reduction of the ZLP tail [1]. For the study of the optical responses of metallic nanomaterials an extremely steep drop of the zero-loss peak is also strongly required for investigations in the very low-loss region down to 0.4 eV [2]. In this paper, we report about both, improvements of the energy resolution and the drop of the ZLP tail. Furthermore we identify, which results depend on the MANDOLINE filter and which results largely do not depend on the MANDOLINE filter, but could also be obtained with the Corrected OMEGA filter.

On the other hand not only the energy resolution determines the analytical capabilities of an energy-filtering TEM (EFTEM) and should be further developed, but also the imaging performance of the energy filter. This was the motivation for the MANDOLINE (magnetic aberration-free noticeably dispersive Omega-like inhomogeneous energy) filter, which was proposed by Uhlemann and Rose [3] and developed by Zeiss within the publicly funded SESAM (sub-electronvolt sub-Ångström microscope) project [4]. Thus we report on this highly sophisticated in-column imaging energy filter, which provides full third-order aberration correction in the spectrum plane. We will discuss in detail its transmissivity and isochromaticity, which besides an improved energy resolution are the most important electron optical parameters for high-end EFTEM and energy-filtered STEM [5] applications. The required transmissivity for different applications is explored in [6], where the additional possibilities due to the exceptionally high transmissivity of the MANDOLINE filter are illustrated.

2. Instrumental setup

The TEM column of the SESAM, shown in Fig. 1 is that of a LIBRA® 200 MC (LIBRA® 200 with monochromator) with a

* Corresponding author. Tel.: +49 7364 203 185.
E-mail address: essers@smt.zeiss.com (E. Essers).

0304-3991/$ - see front matter © 2010 Elsevier B.V. All rights reserved.
doi:10.1016/j.ultramic.2010.02.009

MANDOLINE filter instead of a Corrected OMEGA filter. From top to bottom the microscope consists of a Schottky-type field emission gun (FEG) and the monochromator (MC), which were developed by CEOS for Zeiss. Furthermore it consists of a Koehler illumination system, a condenser objective lens with eucentric goniometer, projector lens systems above and below the in-column filter, and various detectors below the filter, which can be used for energy filtered results: 2k × 2k slow-scan CCD, on-axis TV rate camera, image plates /photographic film, HAADF detector / bright field detector, and beam-stop. An additional high angle annular dark field (HAADF) detector just above the MANDOLINE filter allows for the simultaneous acquisition of EEL spectra and a Z-contrast STEM image (STEM-EELS spectrum imaging), while the HAADF detector below the in-column filter allows for energy-filtered STEM images (e.g. [5]).

As proposed in [7], the projector system below the in-column filter consists of three round lenses. It images either the achromatic image or the spectrum on the detector, thereby magnifying them with a variable post-filter magnification. This variable post-filter magnification of in-column-filters allows one to make optimum use of the filter's transmissivity [6]. Moreover it allows for visual inspection of the EEL spectrum and the imaging and diffraction conditions directly on the viewing screen.

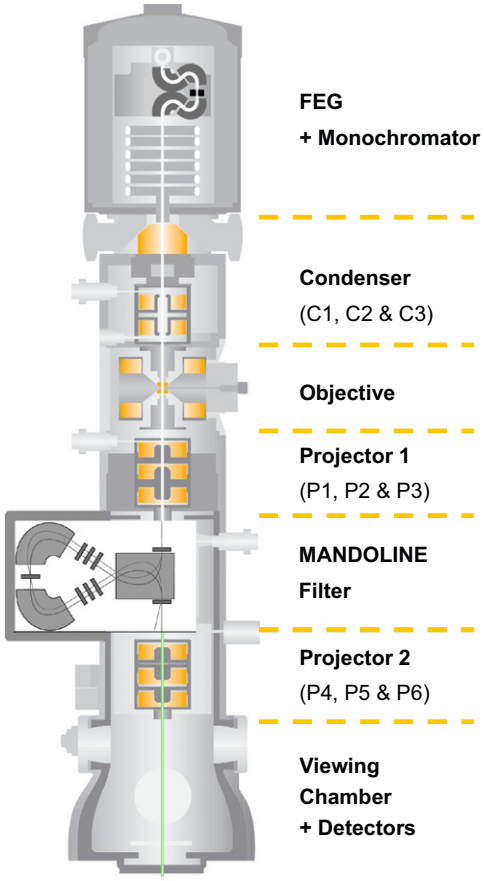

Fig. 1. The TEM column of the SESAM is that of a LIBRA® 200 MC with a MANDOLINE filter instead of a Corrected OMEGA filter.

2.1. Monochromator

The electrostatic Omega-type monochromator [8–11] shown in Fig. 2a and b provides a dispersion of up to 12.4 μm/eV (at 4 kV extractor voltage) at the slit in the symmetry plane [12]. Due to the symmetry of the fundamental rays the dispersion disappears below the monochromator, which is advantageous for both illumination modes. At spot illumination it prevents broadening of the effective source by the dispersion and at TEM illumination it precludes any complications, which are due to rainbow illumination [13]. Furthermore half of the second-order aberrations are cancelled out by symmetry [8]. Electrostatic hexapole fields, which are produced by the shape of the monochromator's electrodes, further reduce the remaining second-order aberrations. The remaining second-order aberrations are sufficiently small, that they actually do not lead to a source broadening. Thus the monochromator design is optimally suited for analytical purposes and allows for high resolution analysis with ultimate energy resolution, since a high beam current can be transferred through a small energy slit width and the spot size is preserved.

An exchangeable gun lens aperture can be chosen from amongst eight sizes starting at 37.5 microns and continuing in steps of $\sqrt{2}$. The gun lens aperture is integrated in the gun to limit the beam current to the used portion in order to minimize broadening of the beam and energy broadening by electron–electron interaction. Moreover for the same purpose all real intermediate images of the source within the monochromator are astigmatic, while the virtual final crossover image at the monochromator's exit is stigmatic. The multi-slit array of the monochromator consists of 10 energy selection slits with a size between 0.5 and 5 μm. Furthermore a 60 μm slit enables the usage of the unfiltered electron beam. By selecting one of the eleven slits of the multi-slit array the energy width of the

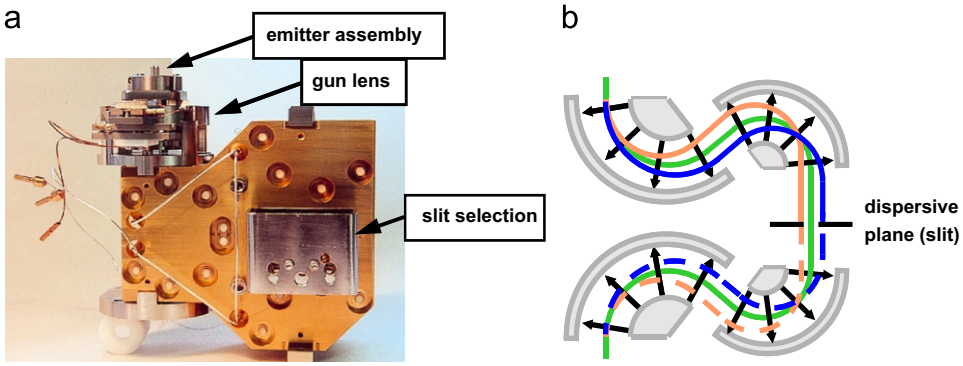

(Courtesy M. Haider, CEOS)

Fig. 2. Electrostatic Omega-type monochromator. (a) Photograph and (b) schematic setup. The energy selection from electrons of different energies is performed by the slit aperture in the symmetry plane.

primary beam can be chosen. This slit choice can be performed mechanically by means of a piezo element. Alternatively the choice of the slit size can be changed quickly and easily electron optically. Any energy resolution (i.e. slit size) can be used with any condenser setting and at any magnification.

With the 60 μm slit (i.e. the beam current is not reduced) the brightness is preserved by the monochromator and has been measured with a LIBRA® 200 MC to be 1.1×10^9 A/(sr cm^2) at 200 kV. For all other slit sizes the monochromator reduces the beam current (and thereby also the brightness) by removing the electrons, which are not in the desired energy range. At an energy resolution of 220 meV, a brightness of 2.3×10^8 A/(sr cm^2) has been measured with a LIBRA® 200 MC at 200 kV. Even though the brightness could be increased by the usage of a Schottky emitter with a smaller tip radius, this would worsen the energy resolution of the unmonochromized beam, as mentioned in 3.1.1.

2.2. Koehler illumination system with monochromator

The electron beam is shaped by the principal optical elements of the illumination system in the following manner: After leaving the Schottky-type electron gun, the electron beam is limited by the gun lens aperture and is focused to a line focus parallel to the slit in the energy selection plane, where the energy selection is carried out. The lower half of the monochromator generates a rotationally symmetric beam without dispersion, which is focused by the accelerator lens into the round gun crossover (CO). The condenser lens system performs Koehler illumination [14] by transferring the CO image onto the front focal plane of the objective prefield lens for TEM illumination. Besides its high flexibility two main advantages of the Koehler illumination are that the intensity over the illumination field is uniform and the ray paths of the incident electrons are parallel. This is highly desirable for diffraction applications and for high resolution imaging. Furthermore switching between the TEM and STEM mode is comfortably realized by changing the current of a single lens without any realignment.

For nano-diffraction and STEM applications the spot mode is used, where the condenser system focuses the gun CO with variable magnification onto the entrance image plane of the objective prefield lens, which produces a strongly demagnified image of the CO in the specimen plane. In combination with the high brightness of the FEG, the improved energy resolution of the monochromator can be used for analytical investigations on the atomic scale.

2.3. MANDOLINE filter

While for the originally proposed version of the MANDOLINE filter [3] an optimization of the third-order aberrations was already planned, the realized version provides full third-order aberration correction in the spectrum plane. Fig. 3a and b shows the setup and the ray path of the MANDOLINE filter. The filter consists of nine symmetrically arranged correction elements, one magnet with a homogeneous field, and two symmetrically arranged magnets with inhomogeneous fields, focusing the ray continuously in both principal sections. Magnets with conical pole faces and inhomogeneous fields are well known from accelerator physics, but their usage in a corrected imaging energy filter is new and more demanding. Higher precision is necessary because of the smaller dimensions and the distortion free imaging in a TEM. In the MANDOLINE filter this is taken into account by the mechanical precision of the realized conical pole faces, which is comparable to the precision of the plane pole faces used in the magnet with the homogeneous field.

Despite the high dispersion (D^*=6.8 μm/ eV at the spectrum plane) and extraordinary transmissivity and isochromaticity, the MANDOLINE filter enlarges the TEM column by only 228 mm due to the intersecting optical axis in the filter. The main advantage of the high dispersion is the availability of small energy selection slits. Furthermore the high dispersion results in a reduced spectrum–diffraction mixing and spectrum–image mixing, which allows a reduced pre-filter magnification. Thus for the same total magnification a higher post-filter magnification can be used in the imaging mode and diffraction mode, thereby reducing the non-isochromaticity at the camera. The high dispersion of the MANDOLINE filter also results in a higher dispersion at the slow-scan CCD (SSCCD) camera, which is nice to have, but does hardly affect the attainable energy resolution, since the lower projective system allows a sufficiently large dispersion at the SSCCD already in combination with the corrected OMEGA filter, as can be seen in 3.1.2. The conditions under which the higher dispersion leads to an improved drop of the zero-loss peak will be discussed in 3.1.3.

Unlike other imaging energy filters, the MANDOLINE filter's design includes external quadrupole fields at the first and the last correction element, which serve for focusing in the non-dispersive direction at the entrance of the first magnet and the exit of the last magnet. This avoids a strongly inclined entrance of the first magnet and exit of the last magnet and makes it possible to arrange correction elements close to the filter's entrance image plane and achromatic image plane, thus simplifying the alignment strategy.

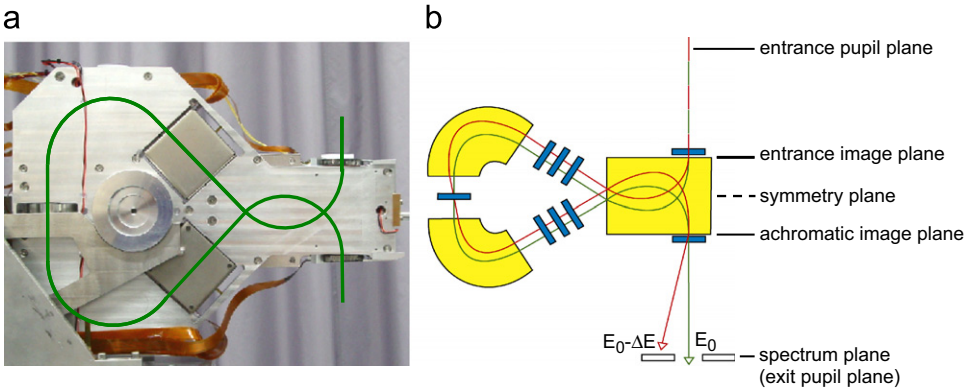

Fig. 3. Setup and ray path of the MANDOLINE filter. (a) Photograph and (b) schematic setup. In the ESI mode the energy selection of electrons of different energies is performed by the slit aperture in the spectrum plane.

3. Experimental results and discussion

3.1. Energy resolution of the monochromator

The overall energy resolution is mainly determined by the monochromator and by the stabilities of the high voltage and the filter current. Furthermore energy broadening due to the Boersch effect has to be avoided, which is achieved by the used monochromator design without stigmatic crossover. Additionally small gun lens apertures are advantageous for energy resolutions below 70 meV.

Contrary to an often encountered belief, the energy resolution for small analyzed areas is usually not limited by the electron optical design of the energy filter; e.g. for a field of view, which corresponds to 23 mm in diameter at the SSCCD, a Corrected OMEGA filter allows almost the same energy resolution as a MANDOLINE filter, as will be shown in 3.1.2.

With the exception of Fig. 6, all results shown in this article were performed at 200 kV with the SESAM, which is a prototype for the LIBRA® 200 MC with respect to the extreme stability of the high voltage and the filter current, while the rest of the electronics is identical. Additionally the spectra in Fig. 6 have been taken with the LIBRA® 200 MC (with the current standard stability of the high voltage and the filter current) to ensure the principal transferability of the results from the SESAM to the LIBRA® 200 MC as will be explained in 3.1.2. All spectra show zero-loss peaks without specimen in order to test the instrumental capabilities.

3.1.1. Characterization of the monochromized ZLP

Fig. 4a shows a comparison of an unmonochromized zero-loss peak (in the background) with a monochromized zero-loss peak for 1.5 μm monochromator slit width. Both spectra were recorded with identical microscope parameters. The full width at half maximum (FWHM) of the monochromized spectrum is 126 meV. Ideally a monochromator would cut out from the unmonochromized spectrum just the region, which is limited by the dashed lines. How close the real spectrum comes to this ideal situation, can be described by the edge steepness or rather by its inverse, defined by the energy difference between the points with 90 and 10% of the maximum intensity. This is demonstrated in Fig. 4b, where for the monochromized spectrum of Fig. 4a an energy difference of 44 meV between 90 and 10% intensity is measured. In this example the attainable FWHM is obviously mainly limited by the slit width of the monochromator and the spectrum even shows a plateau, which is close to the ideal appearance. Taking into account the possibility of deconvolution of the spectra [15], the energy difference between 90 and 10% intensity is even a better indicator of the potential energy resolution of monochromized spectra than the FWHM. If the energy resolution is limited mainly by the monochromator's slit width, this leads to highly reproducible results and enlarges the improvement, which is achievable by deconvolution techniques.

Fig. 4c shows a monochromized zero-loss peak for 0.5 μm monochromator slit width in comparison to the unmonochromized zero-loss peak, both recorded with identical microscope parameters. The monochromized spectrum shows a FWHM of 48 meV and an energy difference of 35 meV between 90 and 10% intensity.

Ideally the monochromized zero-loss peak would have the same height as the unfiltered zero-loss peak, from which it is cut out. This is particularly demanding at good energy resolution. For 126 meV FWHM the monochromized zero-loss peak in Fig. 4a has the same height as the unfiltered zero-loss peak and even for 48 meV FWHM in Fig. 4c the height of the zero-loss peak drops only by 16%.

By removing all electrons, which are not in the desired energy range, even an ideal monochromator inevitably reduces the beam current. Therefore the appropriate energy resolution (monochromator slit width) should be chosen for each experiment. Choosing a much better energy resolution than required, would reduce the beam current needlessly. Removing the electrons, which are not in the energy range of the FWHM of the unmonochromized beam, already reduces the beam current by a third. Compared to this, the beam current is reduced to a quarter in Fig. 4a (126 meV FWHM) and to an eleventh in Fig. 4c (48 meV FWHM). These fractions could be further improved by using a Schottky emitter with a larger tip radius, which would reduce the FWHM of the unmonochromized beam. However, this would also reduce the aforementioned values of the brightness of the FEG, which have been measured with the same tip radius as the spectra in Fig. 4. Therefore a trade-off between brightness and the FWHM of the unmonochromized beam is necessary.

3.1.2. Energy resolution

Fig. 5a, b and c shows the energy resolution of the zero-loss peak for different exposure times. For 0.1 s exposure time Fig. 5a shows an energy resolution of 43 meV (FWHM) and an energy difference of 34 meV between 90 and 10% intensity. This

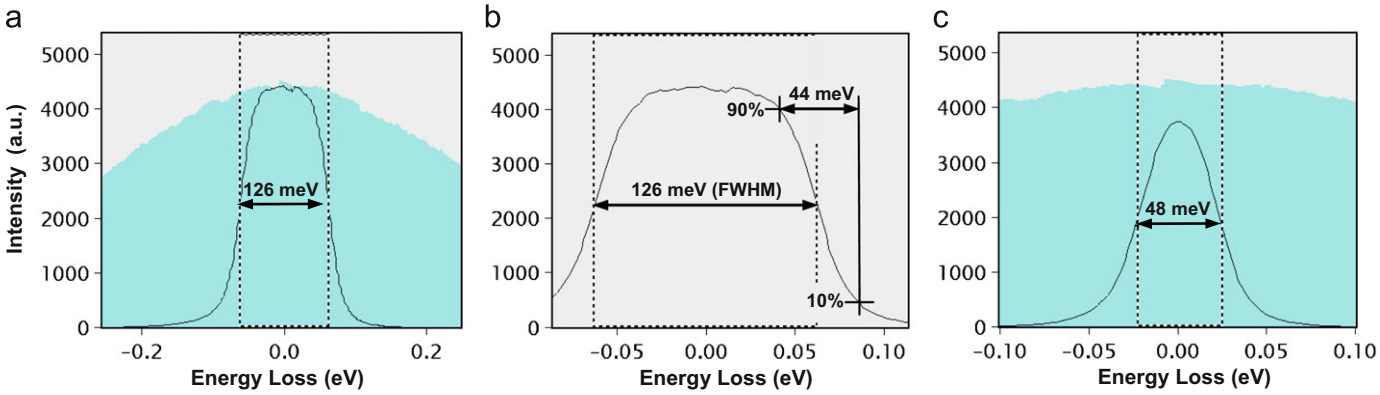

Fig. 4. (a) Comparison between an unmonochromized (in the background) and a monochromized zero-loss peak with identical microscope parameters for both spectra. The monochromized spectrum shows a plateau and 126 meV FWHM, which is limited by the monochromator slit width of 1.5 μm. (b) The inverse of the edge steepness, measured by the energy difference (44 meV) between the points with 90 and 10% of the maximum intensity is a useful indicator for the quality of the monochromized spectrum. (c) Even for 48 meV FWHM the maximum of the monochromized spectrum (taken with 0.5 μm monochromator slit width) is only 16% below the maximum of the unmonochromized spectrum (in the background). Both spectra were taken with identical microscope parameters. In the monochromized spectrum the energy difference between the points with 90 and 10% of the maximum intensity is 35 meV.

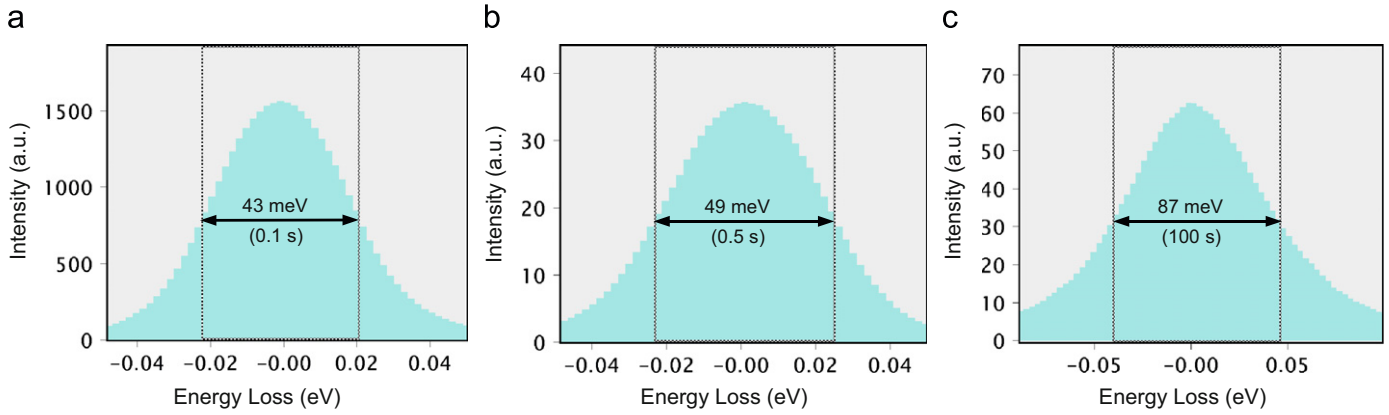

Fig. 5. Energy resolution of the zero-loss peak for different exposure times taken with the MANDOLINE filter at 200 kV. (a) 0.1 s exposure time: 43 meV (FWHM) and an energy difference of 34 meV between 90 and 10% intensity. (b) 0.5 s exposure time: 49 meV (FWHM) and an energy difference of 36 meV between 90 and 10% intensity. For short exposure times, the energy resolution is mainly limited by the energy window width of the monochromator slit, which is 40 meV for all three spectra. (c) 100 s exposure time: 87 meV (FWHM) and an energy difference of 82 meV between 90 and 10% intensity.

spectrum is a sum of 30 spectra, which were recorded, each with 0.1 s exposure time and were aligned [16]. All other spectra in this paper are recorded as a single exposure and presented as raw data. For 0.5 s exposure time Fig. 5b shows an energy resolution of 49 meV (FWHM) and an energy difference of 36 meV between 90 and 10% intensity. Taking into account that the energy window width of the monochromator slit is 40 meV in Fig. 5, it can be concluded, that for short exposure times (together with the extreme stability of the high voltage and the filter current) the energy resolution is mainly limited by the energy window width of the monochromator, thus offering the potential for a substantial improvement by deconvolution techniques. Furthermore it can be concluded from Fig. 5a, that the energy resolution is not affected by the Boersch effect. This is due to the monochromator design and the second smallest (53 micron) gun lens aperture, which has been used for the spectra in Fig. 5, Fig. 7 and Fig. 9.

For 100 s exposure time Fig. 5c shows an energy resolution as good as 87 meV (FWHM) and an energy difference of 82 meV between 90 and 10% intensity, which demonstrates the stability of both the high voltage and the filter current. The spectrum in Fig. 5c was recorded with a dispersion of 340 ch/eV, whereas the spectra in Fig. 5a and b were recorded with a dispersion of 520 ch/eV.

Furthermore we performed two measurements with the Corrected OMEGA filter. In the first measurement we determined experimentally, which energy resolution is in principle possible at 200 kV with a LIBRA® 200 MC (with the current standard stability of the high voltage and the filter current) for an exposure time of 0.03 s. Fig. 6a demonstrates an energy resolution of only 41 meV (FWHM), which has been achieved without deconvolution for 0.03 s exposure time with a dispersion of 125 ch/ eV and a monochromator slit width of 30 meV. (The increased dispersion of the monochromator is achieved by non-standard operation conditions of the FEG.) The microscope was equipped with a 2k × 2k SSCCD camera (14 μm pixel size) and without sheet film camera, which reduces the maximum dispersion at the SSCCD camera by 12% compared to a setup with a sheet film camera. The energy difference between 90 and 10% intensity is 52 meV in Fig. 6a. At first sight it may seem contradictory that the spectrum of Fig. 6a in comparison to those of Fig. 5a and b shows a better energy resolution (FWHM) but an inferior energy difference between 90 and 10% intensity. In fact this is not surprising, but it is due to two factors. Firstly the monochromator energy slit width, which is mainly limiting the energy resolution, is 10 meV larger in Fig. 5 than in Fig. 6a, and secondly the dispersion is much smaller in Fig. 6a than in Fig. 5, thereby enlarging the influence of the detector's point spread function, which is not removed by deconvolution. Due to the different experimental conditions (monochromator energy slit width, exposure time, dispersion, stabilities of the high voltage and the filter current) the results of Fig. 5 are not directly comparable to those of Fig. 6a. Nevertheless the excellent energy resolution of 41 meV demonstrates clearly the potential of the Corrected OMEGA filter.

In a second measurement, we tested the energy resolution of a LIBRA® 200 MC (with the current standard stability of the high voltage and the filter current) at 80 kV for an exposure time of 50 s. Fig. 6b demonstrates an energy resolution of only 77 meV with a monochromator slit width of 40 meV and a dispersion of 97 ch/eV (using a 4k × 4k SSCCD camera with 15 μm pixel size). Fig. 6c shows for the same spectrum the energy difference between 90 and 10% intensity to be 66 meV. Except for the smaller dispersion, the conditions in Fig. 6b and c are very similar to those in Fig. 5. Thus it is impressive to see that for long exposure times at 80 kV the (absolute) stability of the high voltage and the filter current of the LIBRA® 200 MC is already as good as the extreme stability of the high voltage and the filter current of the SESAM at 200 kV.

Since the FWHM corresponds to only 5 channels in Fig. 6a and 7 channels in Fig. 6b, respectively, we use a linear interpolation, which reduces the imprecision for the measurement of the FWHM from 1 channel (8 meV in Fig. 6a and 12 meV in Fig. 6b) to far below 1 meV. For the linear interpolation we refer to the count numbers (representing the intensity), which are shown in Fig. 6b. $N_{(\max)}$ is the count number of the channel with the most counts (i.e. the maximum of the zero-loss peak). At the left hand side and the right hand side of the zero-loss peak the count numbers of the neighboring channels to 50% $N_{(\max)}$ are denoted by $N_{(l.b.50\%)}$ (left, below 50%), $N_{(l.a.50\%)}$ (left, above 50%), $N_{(r.b.50\%)}$ (right, below 50%), and $N_{(r.a.50\%)}$ (right, above 50%). The FWHM in Fig. 6b can be divided into three parts: a 6 channel (a=6) wide region between $N_{(l.a.50\%)}$ and $N_{(r.a.50\%)}$ in the middle and two small regions, where the liner interpolation is carried out between $N_{(l.b.50\%)}$ and $N_{(l.a.50\%)}$ on the left and between $N_{(r.b.50\%)}$ and $N_{(r.a.50\%)}$ on the right. Accordingly the number $n_{(FWHM)}$ of channels that corresponds to the FWHM is given by

$$n_{(FWHM)} = \left|\frac{N_{(l.a.50\%)} - 0.5 \times N_{(\max)}}{N_{(l.a.50\%)} - N_{(l.b.50\%)}}\right| + a + \left|\frac{N_{(r.a.50\%)} - 0.5 \times N_{(\max)}}{N_{(r.a.50\%)} - N_{(r.b.50\%)}}\right|. \quad (1)$$

For Fig. 6b (with 97 ch/eV) this results in $n_{(FWHM)}$=0.98+6+0.45=7.43, which corresponds to a FWHM of 77 meV, while for

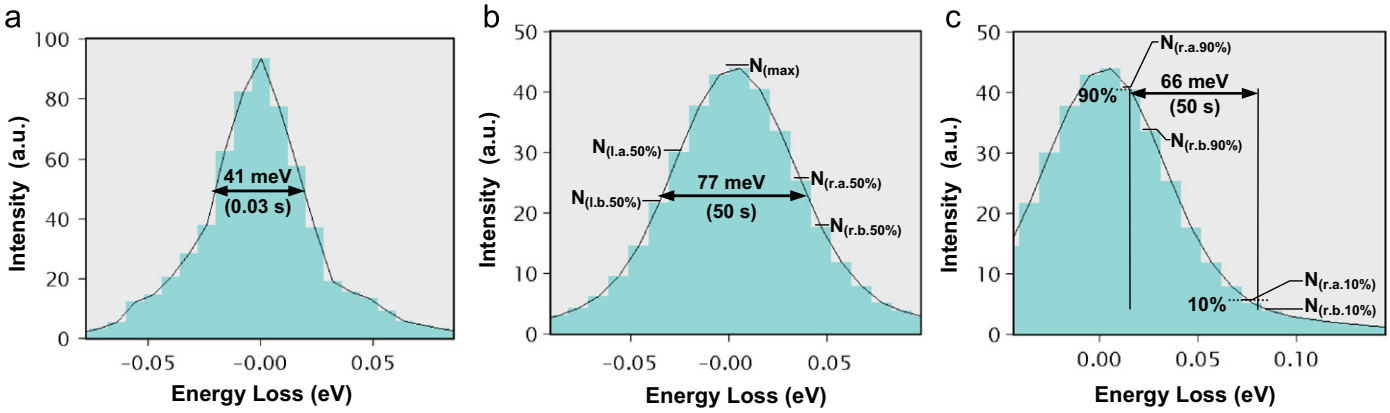

Fig. 6. Energy resolution of the zero-loss peak for different exposure times taken with the corrected OMEGA filter. (a) A FWHM of 41 meV (5.16 channels) has been attained for 0.03 s exposure time at 200 kV with a monochromator slit width of 30 meV. (b) For 50 s exposure time a FWHM of 77 meV (7.43 channels) has been attained at 80 kV with a monochromator slit width of 40 meV. The FWHM is calculated by linear interpolation with Eq. (1). (c) The same spectrum shows an energy difference of 66 meV between 90 and 10% intensity as calculated by linear interpolation with Eqs. (2) and (3). This demonstrates, that the (absolute) stability of the high voltage and the filter current of the LIBRA® 200 MC at 80 kV for long exposure times is already as good as the extreme stability of the high voltage and the filter current of the SESAM at 200 kV.

Fig. 6a (with 125 ch/eV) it results in $n_{(FWHM)}$=5.16, which corresponds to a FWHM of 41 meV.

In a similar way a linear interpolation is used for the measurement of the energy difference between 90 and 10% intensity for the spectra of Fig. 6a and c. Fig. 6c shows the count numbers of the neighboring channels to 90% $N_{(\max)}$, which are denoted by $N_{(r.a.90\%)}$ (right, above 90%) and $N_{(r.b.90\%)}$ (right, below 90%) and the neighboring channels to 10% $N_{(\max)}$, which are denoted by $N_{(r.a.10\%)}$ (right, above 10%), and $N_{(r.b.10\%)}$ (right, below 10%). Again there are three regions: a 5 channel (b_r=5) wide region between $N_{(r.b.90\%)}$ and $N_{(r.a.10\%)}$ in the middle and two small regions, where the liner interpolation is carried out between $N_{(r.a.90\%)}$ and $N_{(r.b.90\%)}$ and between $N_{(r.a.10\%)}$ and $N_{(r.b.10\%)}$. Accordingly the number $n_{r(90\%-10\%)}$ of channels that corresponds to the energy difference between 90 and 10% intensity is given for the right hand side of the spectrum by

$$n_{r(90\%-10\%)} = \left|\frac{0.9\times N_{(\max)} - N_{(r.b.90\%)}}{N_{(r.a.90\%)} - N_{(r.b.90\%)}}\right| + b_r + \left|\frac{N_{(r.a.10\%)} - 0.1\times N_{(\max)}}{N_{(r.a.10\%)} - N_{(r.b.10\%)}}\right|. \quad (2)$$

For Fig. 6c this results in $n_{r(90\%-10\%)}$=0.86+5+0.61=6.47. In the same way the number $n_{l(90\%-10\%)}$ of channels that corresponds to the energy difference between 90 and 10% intensity for the left hand side of the spectrum has been measured to be $n_{l(90\%-10\%)}$=6.31 by replacing each "*r*" in Eq. (2) by an "*l*". The slight difference between the values for the right hand side and the left hand side is taken into account for all energy differences between 90 and 10% intensity in this paper by using the mean value

$$n_{(90\%-10\%)} = 0.5\times(n_{r(90\%-10\%)} + n_{l(90\%-10\%)}). \quad (3)$$

Herewith the energy difference between 90 and 10% intensity results in 66 meV in Fig. 6c and 52 meV for the spectrum of Fig. 6a.

Now we want to confirm our statement that the energy resolution is mainly determined by the monochromator and by the stabilities of the high voltage and the filter current and does not depend on the MANDOLINE filter. For this purpose we compare the results of Fig. 5 with the energy resolution that would have been achieved upon replacing the MANDOLINE filter by a Corrected OMEGA filter. While the susceptibility to stray fields and vibrations is uncritical for both filters, there are two main differences between the filters, which influence the energy resolution and therefore have to be taken into account. These are the non-isochromaticity and the dispersion. (The magnification of the lower projective system is the same for both filters.)

The influence of the larger non-isochromaticity can be calculated accurately and it turns out that it would hardly affect the energy resolution in Fig. 5a, b and c, which are taken with a field of view that corresponds to 23 mm in diameter on the SSCCD. Over this field of view, the non-isochromaticity of the Corrected OMEGA filter has a root mean square deviation of only 8 meV, as measured from experimental data. Thus the broadening of the energy resolution due to the larger non-isochromaticity (calculated by taking the root of the sum of squares) would be 1 meV if the energy resolution were 32 meV. For an energy resolution of more than 32 meV, the broadening would be even less than 1 meV.

The influence, which the smaller dispersion would have on the energy resolution in Fig. 5 cannot be taken into account so easily. The dispersion of the Corrected OMEGA filter is 1.85 μm/eV (at 200 kV) instead of the 6.8 μm/eV with the MANDOLINE filter. There are three effects caused by this reduction of the dispersion by a factor of 3.7. Firstly spectrum–diffraction mixing must be avoided more carefully, which has no influence in the case of Fig. 5, since the spectra are taken with high magnification. Secondly at the smaller dispersion the FWHM is not measured with a satisfying precision, thus resulting in a large error bar for the measurement. This imprecision can easily be overcome by linear interpolation, as shown in Fig. 6b. The third effect of the reduced dispersion is an energy broadening due to the point spread function (PSF) of the detector. Taking into account all these effects, the energy resolution is expected to be 44 meV in Fig. 5a, 50 meV in Fig. 5b, and 87 meV in Fig. 5c upon replacing the MANDOLINE filter by a Corrected OMEGA filter, if the PSF is removed by deconvolution.

Although the broadening of the energy resolution due to the PSF theoretically can be removed by deconvolution, it is also interesting to know the energy broadening without deconvolution. Therefore we will derive from Fig. 6a an upper limit for the energy broadening due to the PSF. The broadening of the energy resolution is calculated (by taking the root of the difference of squares) from the measured FWHM of 41 meV and the energy slit width of 30 meV. Even though this broadening of the energy resolution originates from the accumulated effects of the PSF and the instabilities of the high voltage and the filter current, in an extremely conservative approach this accumulated energy broadening can be considered as an upper limit for the energy broadening due to the PSF. With this experimentally verified

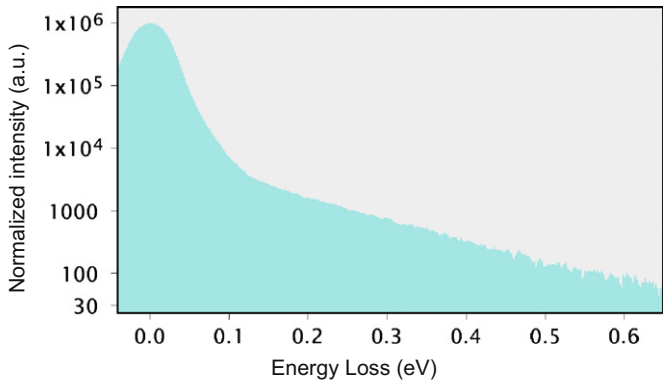

Fig. 7. Logarithmic plot of an EEL spectrum (maximum scaled to 10^6) taken with 0.1 s exposure time with the MANDOLINE filter at 200 kV. The zero-loss peak drops by 10 after 48 meV, 10^2 after 91 meV, 10^3 after 260 meV, and 10^4 after 570 meV. This extreme steep drop of the monochromized zero-loss peak establishes ideal preconditions for band gap measurements and investigations in the very low-loss region.

upper limit it is ensured, that without deconvolution the energy resolution would be less than 52 meV in Fig. 5a, less than 56 meV in Fig. 5b, and less than 92 meV in Fig. 5c upon replacing the MANDOLINE filter by a Corrected OMEGA filter (with a monochromator energy slit width of 40 meV).

A less stringent but probably more realistic estimation of the expected energy broadening due to the reduced dispersion and the detector's PSF can be achieved by a comparison with the literature. With the Corrected OMEGA filter the maximum dispersion at the SSCCD camera is between 125 and 141 ch/eV, which would result in 5-6 channels for 43 meV (FWHW), 6-7 channels for 49 meV (FWHM), and 11-12 channels for 87 meV (FWHM) for the spectra of Fig. 5. In [17] a change of the dispersion by a factor of 10, which corresponds to a change of the FWHM from 47 channels to 5 channels, give rise to an increase of the FWHM of 6%. Based on this, the energy resolution is expected to be 47 meV in Fig. 5a, 53 meV in Fig. 5b, and 89 meV in Fig. 5c upon replacing the MANDOLINE filter by a Corrected OMEGA filter (with a monochromator energy slit width of 40 meV) when no deconvolution is performed.

In summary the degradation of the energy resolution in Fig. 5a, b and c would be less then 1 meV upon replacing the MANDOLINE filter by a Corrected OMEGA filter, if a deconvolution with the PSF of the detector is performed. Without deconvolution the degradation is estimated to be about 4 meV for Figs. 5a and 2 meV for Fig. 5c. With a comparative measurement it has been ensured in an extremely conservative approach that the degradation without deconvolution is less than 9 meV for Fig. 5a and less than 5 meV for Fig. 5c. Thus, for spectroscopic applications a Corrected OMEGA filter provides almost the same energy resolution as the MANDOLINE filter.

3.1.3. Drop of the ZLP tail

Fig. 7 shows a logarithmic plot of an EEL spectrum (maximum scaled to 10^6) taken with 0.1 s exposure time. The zero-loss peak drops by 10 after 48, 10^2 after 91, 10^3 after 260, and 10^4 after 570 meV even without deconvolution. This extremely steep drop of the monochromized zero-loss peak establishes ideal preconditions for band gap measurements and investigations in the very low-loss region. Besides the instabilities of the high voltage and the filter current, the reduction of the ZLP tail is also limited by the tail of the detector's PSF, especially when using a slow-scan CCD camera. Therefore it is expected that the usage of a Corrected OMEGA filter instead of the MANDOLINE filter will compromise the drop of the ZLP, which could be counterbalanced

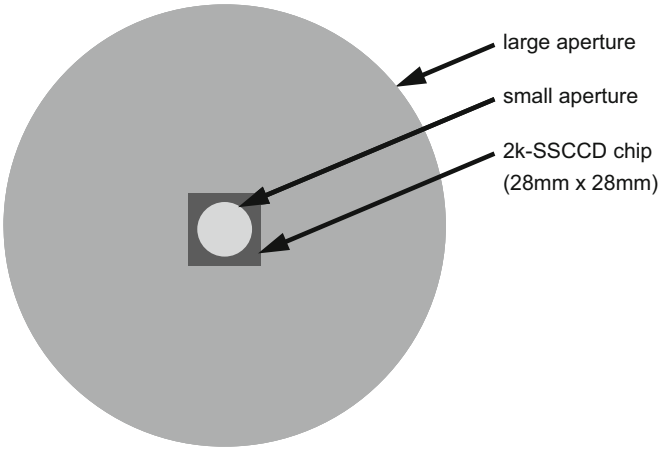

Fig. 8. Comparison of the size between the small filter entrance aperture (inner circle), the large filter entrance aperture (large circle) and the $2k \times 2k$ CCD chip (square, 28×28 mm). With the large aperture of the MANDOLINE filter, which is eight times larger than the small one, a region of 120 mm in diameter on the viewing screen can be illuminated, while the small aperture allows for illuminating a region of 23 mm in diameter on the SSCCD camera.

by deconvolution techniques [17,18] or by using imaging plates, which is easily possible with the sheet film camera in combination with the Corrected OMEGA filter or MANDOLINE filter.

3.2. Imaging properties of the MANDOLINE filter

As already indicated, the energy resolution for a small filter entrance aperture does not require the MANDOLINE filter, but originates from the monochromator and the stability of the high voltage and the filter current. The spectra in Fig. 5 were taken with a small filter entrance aperture, which is depicted in Fig. 8 (as inner circle) in the imaging mode in comparison to a large aperture (large circle) and the $2k \times 2k$ CCD chip (square, 28×28 mm). With the large aperture, which is eight times larger than the small one, a region of 120 mm in diameter on the viewing screen can be illuminated, while the small aperture allows for illuminating a region of 23 mm in diameter on the SSCCD camera. An EEL spectrum taken with the large filter entrance aperture and 0.1 s exposure time is shown in Fig. 9. It demonstrates an energy resolution of only 52 meV (FWHM), which is still mainly limited by the energy slit width of the monochromator of 40 meV. This proves impressively the excellent isochromaticity (i.e. small non-isochromaticity) of the MANDOLINE filter.

3.2.1. Isochromaticity

The non-isochromaticity is caused by remaining higher-order aberrations of the filter in the spectrum plane. Electrons which have the same energy, but come from different positions in the image plane are focused at slightly different positions in the spectrum plane and it thus appears as if the electron energies would differ from each other. Therefore the spectra of off-axis image points are shifted with respect to the spectra of axial image points in general. For the MANDOLINE filter, the energy shift over the field of view is dramatically reduced compared to all other imaging energy filters. This results in non-isochromaticity maps in the range below 10 meV, thus ensuring that the non-isochromaticity is without effect for any applications. The outstanding isochromaticity of the MANDOLINE filter is shown in Fig. 10, where the non-isochromaticity is measured to be less than 5 meV over the whole 24×24 mm CCD chip. The excellent

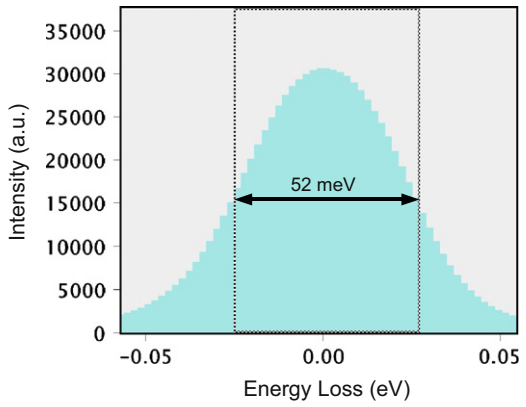

Fig. 9. Zero-loss peak recorded with the large filter entrance aperture and 0.1 s exposure time with the MANDOLINE filter at 200 kV. The energy difference between 90 and 10% intensity is 39 meV. The energy resolution of only 52 meV (FWHM) is mainly limited by the energy window width of the smallest monochromator slit, which is 40 meV. This demonstrates the excellent isochromaticity of the MANDOLINE filter even for a large field of view.

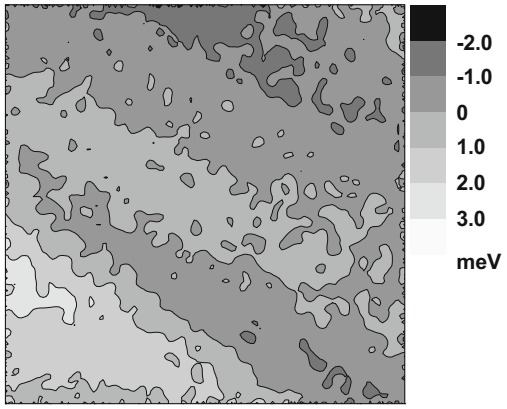

Fig. 10. Isochromaticity of the MANDOLINE filter. The greyscales/colours in the picture show how the energy of the electrons seems to change over the field of view. (This is the effect of the non-isochromaticity.) The non-isochromaticity is measured to be less than 5 meV over the whole 24 × 24 mm CCD chip.

isochromaticity is essential for all kinds of small energy window imaging applications, which are described in the following.

3.2.2. EFTEM spectrum imaging with improved energy resolution

Corrected imaging energy filters offer a range of applications, which demand an improved energy resolution for EFTEM spectrum imaging, such as the mapping of bonding states and plasmon energy mapping [2,19,20]. Such applications are usually performed as STEM-EELS spectrum imaging, which is possible with the HAADF detector just above the MANDOLINE filter, thereby taking a spectrum at each image point as usually realized in dedicated STEMs. This has the advantage of a high energy resolution, but the drawback of a strongly limited number of image points due to the required acquisition time. The alternative approach is EFTEM spectrum imaging, which produces many more image points, but usually has the drawback of a reduced energy resolution due to the slit width of the energy selection slit. Due to the high dispersion of the MANDOLINE filter, 0.2 eV energy slits are available in good quality, thus producing a homogeneous intensity over the whole image field. Thus EFTEM spectrum imaging with very good energy resolution is enabled by the MANDOLINE filter. Due to the outstanding transmissivity this high energy resolution EFTEM spectrum imaging can be performed for a large field of view (e.g. ∅ 2.2 μm at 5 mrad and an energy slit width of ΔE=0.2 eV). First applications [2,20] indicate, that EFTEM spectrum imaging with improved energy resolution will become an important tool especially for measurements in the low-loss range.

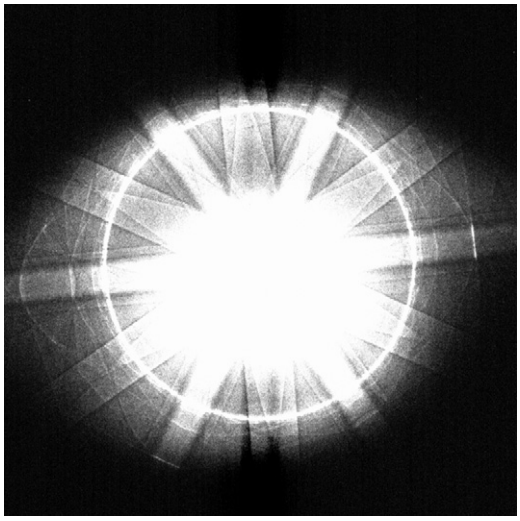

Fig. 11. CBED pattern of Si [1 1 1] taken with the MANDOLINE filter at 200 kV. Scattering angles up to 83 mrad are transferred in all directions through the energy slit width of 0.41 eV. Furthermore the distortion of the MANDOLINE filter is far below 1%. (The measured maximum deviation of the FOLZ ring from a perfect circle is 0.4%.).

3.2.3. CBED and transmissivity

Usually the energy filtering of convergent-beam electron diffraction (CBED) patterns is used to cut off the inelastically scattered electrons. In this way at 5.2 eV energy slit width scattering angles $\alpha_0 > 150$ mrad can be transferred in CBED patterns with the MANDOLINE filter, as demonstrated in [6].

Additionally, CBED patterns can also be used to measure the transmissivity of an imaging energy filter. As an example we use a CBED pattern to prove the transmissivity of the MANDOLINE filter, which was specified in the SESAM project to be at least T=890 nm^2 at 0.5 eV energy slit width. Therefore during the site acceptance test a CBED pattern with only 0.41 eV energy slit width was taken, which is an available slit size close to 0.5 eV. In the CBED pattern of Si [1 1 1] shown in Fig. 11, beyond the first-order Laue zone (FOLZ) ring at 73 mrad, scattering angles up to 83 mrad are transferred in all directions through the energy slit width of 0.41 eV. For an improved visibility despite of the high dynamic range, Fig. 11 shows the square root of the CBED pattern's intensity. Furthermore it can be seen that the distortion of the MANDOLINE filter is far below 1%. (The measured maximum deviation of the FOLZ ring from a perfect circle is 0.4%.)

In the following we derive how the transmissivity can be calculated from a CBED pattern. The transmissivity T of an imaging energy filter is defined [21] as the simultaneously transferred image field with a radius ρ and aperture half-angle α

$$T = (\pi \times \rho \times \alpha)^2. \quad (4)$$

In the case of the third-order corrected MANDOLINE filter the dependence of the transmissivity T on the energy slit width ΔE is

$$\mathrm{T} \sim \Delta E^{2.5} \quad (5)$$

as can be concluded from [21]. For a given energy slit width and field of view, the transmissivity limits the maximum scattering angle that can be transferred through the filter. Alternatively, for a

given energy slit width and scattering angle, it limits the maximum filtered image field.

At first sight, the transmissivity appears not to be a critical parameter in the diffraction mode since the smallest electron energy losses due to plasmon excitations usually have energies of several eV. Furthermore, the analyzed areas are small, which is especially true for CBED where the spot sizes are in the range of 10 nm. Nevertheless, this changes dramatically if the scattering angle exceeds 30 mrad, since then the spherical aberration coefficient C_S of the objective lens has to be taken into account (SESAM: C_S=1.16 mm). Then the plane of least confusion becomes important, since it acts as a pupil plane and should be imaged onto the filter's spectrum plane, which is the energy filter's pupil plane.

The radius δ_S of the spherical aberration disk (of the plane of least confusion) projected onto the specimen is given by

$$\delta_S = C_S \times \alpha^3/4. \tag{6}$$

Together with the transmissivity Eq. (4) and the maximum transferred scattering angle α_{max}, this results in

$$T = \left(\frac{\pi \times C_S \times {\alpha_{max}}^4}{4}\right)^2. \tag{7}$$

This formula allows for the calculation of the transmissivity from diffraction patterns with large scattering angles and in particular from CBED patterns. It presumes that the plane of least confusion is properly imaged onto the filter's spectrum plane. If this condition is not fulfilled, the determined transmissivity will be smaller than the transmissivity of the EFTEM is in reality. Thus this method tends to result in somewhat too small values, especially when not properly carried out. Nevertheless the invaluable advantage of this method is that the object field, scattering angle, and the energy slit width used in calculating the transmissivity are truly those obtained through experiment. This is the crucial point, where other methods for the calculation of the transmissivity can yield too optimistic values by using a scattering angle or energy slit width that was not physically existent during the measurement. If the energy slit width is not physically existent during the measurement (i.e. no energy slit of the given size is inserted during the measurement), this also raises the question, which energy slit width would be required to transfer simultaneously the energy range of the non-isochromaticity figure and the therewith convoluted image of the diffraction pattern (in the imaging mode) or image of the object field (in the diffraction mode). In contrast to that, the calculation by Eq. (7) yields an experimentally proven transmissivity (which may be considerably smaller than the transmissivity values determined by other methods).

For the Si [1 1 1] CBED pattern of Fig. 11 taken at 0.41 eV slit width the transferred angle of 83 mrad results in the outstanding transmissivity of $T_{(0.41\ eV)}$=1870 nm^2 (at 200 kV). Using Eq. (5), we calculate the transmissivity for a 0.5 eV energy slit width to be $T_{(0.5\ eV)}$=3070 nm^2, which surpasses the specification by far. For comparison with other imaging energy filters we calculate with Eq. (5) the transmissivity for a 1 eV energy slit width to be $T_{(1\ eV)}$=17,400 nm^2 (at 200 kV), which is about two orders of magnitude larger than the transmissivity of the Corrected OMEGA filter or the latest post-column filter (GIF QuantumERS^{TM}), when measured with the same method.

The extraordinarily high transmissivity of the MANDOLINE filter allows for electron-spectroscopic imaging (ESI) of large fields of view with energy windows as small as 0.2 eV, thus enabling the applications of EFTEM spectrum imaging with improved energy resolution, mentioned in 3.2.2. Moreover the huge transmissivity allows for band gap mapping [5], the measurement of radial distribution functions, and all other kind of energy filtering applications, which utilize large scattering angles.

4. Conclusions

The energy resolution properties for a small filter entrance aperture are ruled by the monochromator and the stability of the high voltage and the filter current (and not by the MANDOLINE filter), as can be concluded from the comparison of the results taken with the MANDOLINE filter and the Corrected OMEGA filter. For 0.1 s exposure time an energy resolution of 43 meV has been attained in the SESAM at 200 kV with a monochromator slit width of 40 meV. Using a Corrected OMEGA filter instead of the MANDOLINE filter in the same setup (i.e. with extreme stability of the high voltage and the filter current), an energy resolution of 47 meV is expected under the same conditions. Experimentally an energy resolution of 41 meV has been attained for 0.03 s exposure time with the Corrected OMEGA filter (with the current standard stability) at 200 kV with a monochromator slit width of 30 meV. For 50 s exposure time at 80 kV an energy resolution as good as 77 meV has been attained with a LIBRA® 200 MC, whereas for 100 s exposure time an energy resolution of 87 meV has been attained in the SESAM at 200 kV, both of them with a monochromator slit width of 40 meV. This indicates, that at 80 kV for long exposure times the (absolute) stability of the high voltage and the filter current of the LIBRA® 200 MC is already as good as the extreme stability of the high voltage and the filter current of the SESAM at 200 kV.

Concerning the characterization of monochromized spectra, we recommend providing not only the FWHM but also the edge steepness of the ZLP, which indicates the potential for an additional energy resolution improvement by deconvolution of the monochromized spectrum.

Furthermore, the extremely steep drop of the monochromized zero-loss peak by 10^3 after 260 meV and 10^4 after 570 meV, which is attainable in the SESAM even without deconvolution, establishes ideal preconditions for band gap measurements and investigations in the very low-loss region.

Moreover, the benchmark data of the MANDOLINE filter's imaging properties, namely the transmissivity and isochromaticity define a new state of the art for imaging energy filters. We derived how the transmissivity can be calculated from CBED patterns. The resulting outstanding transmissivity of $T_{(1\ eV)}$=17,400 nm^2 of the MANDOLINE filter in combination with its large dispersion of D^*=6.8 μm/eV allow EFTEM spectrum imaging (EFTEM SI) with energy windows $\leq$200 meV and reasonable fields of view, thus opening up new windows for research especially in the low-loss range (e.g. [2,20]). While the non-isochromaticity is often limiting for EFTEM at small slit widths, the MANDOLINE filter's measured non-isochromaticity of less than 5 meV sets no limit for any applications.

Acknowledgments

We gratefully acknowledge H. Rose, F. Kahl, and S. Uhlemann for the concepts and electron optical designs of the monochromator and the MANDOLINE filter, D. Krahl for excellent technical and scientific support, and M. Haider, S. Uhlemann, and E. Schwan for the development of the monochromator. We are grateful for the financial support of the SESAM project by the DFG Germany, the Max Planck Society, and the state Baden-Württemberg. We are indebted to M. Rühle, who founded the SESAM project and P. van Aken, who continues the good cooperation.

References

[1] K. Kimoto, G. Kothleitner, W. Grogger, Y. Matsui, F. Hofer, Micron 36 (2005) 185.
[2] W. Sigle, J. Nelayah, C.T. Koch, P.A. van Aken, Opt. Lett. 34 (2009) 2150.
[3] S. Uhlemann, H. Rose, Optik 96 (1994) 163.
[4] M. Rühle, C. Elsässer, C. Scheu, W. Sigle, Microsc. Microanal. 6 (Suppl. 2: Proceedings) (2000) 188.
[5] L. Gu, W. Sigle, C.T. Koch, J. Nelayah, V. Srot, P.A. van Aken, Ultramicroscopy 109 (2009) 1164.
[6] C.T. Koch, W. Sigle, R. Höschen, M. Rühle, E. Essers, G. Benner, M. Matijevic, Microsc. Microanal. 12 (2006) 506.
[7] H. Rose, Ultramicroscopy 56 (1994) 11.
[8] F. Kahl, Thesis, Technische Universität Darmstadt, 1999 〈http://deposit.ddb.de/cgi-bin/dokserv?idn=960411011〉.
[9] H. Rose, Ultramicroscopy 78 (1999) 13.
[10] F. Kahl, H. Rose, Proceedings of the 12th European Congress on Electron Microscopy, vol. 3, 2000, p. 1459.
[11] S. Uhlemann, M. Haider, Proceedings of the 15th International Congress on Electron Microscopy, vol. 3, 2002, p. 327.
[12] S. Uhlemann, Private communication (2008).
[13] M. Lentzen, A. Thust, Proceedings of the 16th International Congress on Electron Microscopy, vol. 2, 2006, p. 638.
[14] G. Benner, W. Probst, J. Microsc. 174 (1994) 133.
[15] A. Gloter, A. Douiri, M. Tencé, C. Colliex, Ultramicroscopy 96 (2003) 385.
[16] Script provided by C.T. Koch, Max Planck Institute for Metals Research, Stuttgart.
[17] S. Lazar, G.A. Botton, H.W. Zandbergen, Ultramicroscopy 106 (2006) 1091.
[18] J.M. Zuo, Microsc. Res. Tech. 49 (2000) 245.
[19] W. Sigle, S. Krämer, V. Varshney, A. Zern, U. Eigenthaler, M. Rühle, Ultramicroscopy 96 (2003) 565.
[20] J. Nelayah, L. Gu, W. Sigle, C.T. Koch, I. Pastoriza-Santos, L.M. Liz-Marzán, P.A. van Aken, Opt. Lett. 34 (2009) 1003.
[21] S. Uhlemann, H. Rose, Ultramicroscopy 63 (1996) 161.